Experimental Study and Modeling of the g_m-I Dependence of Long-Channel MOSFETs

Michael Cheng
Electrical Engineering Department
California Polytechnic State University
San Luis Obispo, CA, USA

Vladimir Prodanov
Electrical Engineering Department
California Polytechnic State University
San Luis Obispo, CA, USA

***Abstract*—this paper describes an experimental study and modeling of the current-transconductance dependence of the ALD1106 and ALD1107 arrays. The study tests the hypothesis that the I-g_m dependence of these 7.8 µm MOSFETs conforms to the Advanced Compact Model (ACM). Results from performed measurements, however, do not support this expectation. Despite the relatively large length, both ALD1106 and ALD1107 show sufficiently pronounced 'short-channel' effects to render the ACM inadequate. As a byproduct of this effort, we confirmed the modified ACM equation. With an m factor of approximately 0.6, it captures the I-g_m dependence quite well. The paper also introduces several formulas and procedures for I-g_m model extraction and tuning. These are not specific to the ALD transistor family and can be applied to MOSFETs with different physical size and electrical performance.**

***Index Terms*—analog; MOSFET; transconductance; model; ACM**

I. Introduction

In electronic design, transistors find use in multiple circuits. Digital circuits typically use transistors as switches, while analog circuits use them as amplifiers. As an amplifier, the voltage across the gate-source terminals of a MOSFET device changes the current flowing through its source-drain terminals. The transistor is biased at a particular DC operating point to maximize potential small-signal gain. The transconductance, g_m, is the slope of the transfer characteristic of a transistor evaluated at the operating point. For a MOSFET, it is captured as follows:

$$g_m = \left.\frac{di_D}{dv_{GS}}\right|_{o/p.} \tag{1}$$

For a given g_m, the voltage gain of a circuit is found by multiplying g_m with the output resistance of the stage.

The Advanced Compact Model (ACM) models the I-g_m relations of a MOSFET and is valid for long-channel devices. It provides a continuous function between sub-threshold and strong inversion operating regions. According to the ACM [1], the I-g_m expression for a MOSFET in saturation is:

$$g_m = \frac{2}{1+\sqrt{1+I_D/I_S}} * \frac{I_D}{nU_T} \tag{2}$$

The normalization current, I_S, is defined in (3), where U_T is the thermal voltage kT/q. The rest of the quantities have their usual meaning.

$$I_S = \frac{1}{2} n\mu C_{ox} \frac{W}{L} U_T^2 \tag{3}$$

When I_D is much smaller than I_S, the device operates in weak inversion, where the gate transconductance takes the form:

$$g_m = \frac{I_D}{nU_T} \tag{4}$$

When I_D is much larger than I_S, the device operates in strong inversion, where the transconductance is proportional to the square-root of the drain current. However, short-channel MOSFETs behave differently. When the channel length of the transistor is reduced, the channel carrier velocity reaches a limit due to high horizontal electric field values [2]. This effect is only seen at higher currents in strong inversion and manifests itself in a weaker than square-root g_m-I dependence.

According to [3], the impact of strong electric fields can be modeled by replacing the square root in (2) with a larger-value exponent m. This modified equation, which has not been previously experimentally verified, is (5).

$$g_m \cong \frac{2}{1+(1+I_D/I_{norm})^{\mathrm{m}}} \times \frac{I_D}{V_{norm}}, \quad m \geq 0.5 \tag{5}$$

Here V_{norm} equals nU_T, and I_{norm} takes the place of I_S. The modified ACM is attractive because it is simple yet arguably capable of accounting for various levels of 'high-filed' effects.

In this work, we study the behavior of two MOSFETs, ALD1106 and ALD1107, with the goal of demonstrating their I-g_m characteristics conform to (2). Expecting a good agreement with the ACM, we learned that capturing the I-g_m relation needed the modified ACM instead.

Section II discusses data collection and data preprocessing. Section III deals with various aspects of model tuning, and Section IV presents the results.

II. I-V Data Collection and Preprocessing

As stated in the Introduction, we wish to find whether the I-g_m dependence of ALD1106 and ALD1107 obeys (2). This is a valid supposition because both transistors have a channel length of 7.8 µm, implying a 'long-channel' device [2], [4]. The first step of the process is obtaining reliable I-V data that covers the operating range of the device. This includes weak, moderate, and strong inversion.

Our experimental data consists of more than one hundred fifty I-V points per transistor studied. As shown in Table I, the current spans approximately seven decades, and for the n-channel devices (ALD1106), it ranges from 1 nA to 19 mA. The range for the p-channel devices (ALD1107) is somewhat smaller: 1 nA to 6.5 nA. Different maximum currents were

TABLE I: NUMBER OF I-V POINTS PER TRANSISTOR AND THEIR DISTRIBUTION

		1-10 nA	10-100 nA	0.1-1 µA	1-100 µA	0.1-1 mA	Beyond 1 mA
Number of Points	ALD1106	10	10	10	100	10	19 (1 mA step)
	ALD1107	10	10	10	100	10	13 (0.5 mA step)

employed to ensure the gate-source voltage of the FET under test does not exceed the 10.6 V limit defined by the manufacturer [5], [6].

The I-V points are pseudo-logarithmically spaced in the current domain with ten uniformly distributed points within each decade. An exception is the 1-to-100 µA range, where we took 100 as opposed to 20, to better capture transistor transition from weak to strong inversion.

All data were obtained using a diode-connected transistor configuration, where the Keithley-2400 serves as a current source to bias the transistor under test. Fig. 1a and 1b show the test setup. The Keithley supplies the drain current and simultaneously measures the V_{GS} of the device, so no additional hardware is needed.

Extracting I-V data from a diode-connected device is attractive because the setup is simple and the connection keeps the MOSFET in saturation. The disadvantage of the 'diode-connection' is that the change in I_D is due to changes in both V_{GS} and V_{DS}. This means that the derivative of the drain current with respect to V_{GS} yields the sum of g_m and g_{ds}. Attributing the change to g_m alone, results in an error. The error, however, is relatively small because the g_m is typically much larger than g_{ds}. This is notably true for devices meant for analog applications.

There are at least two phenomena that could compromise the validity of the data gathered: thermal heating and noise. The thermal heating, a concern at high currents, was addressed by an automated data collection scheme. A LabView program controlled the pseudo-logarithmic current sweep and collected gate-source voltage measurements, reducing the time the MOSFET spends in a high-current regime. Minimizing heating is essential because thermal effects manifest in a manner similar to high-field effects: the I_D and the g_m are reduced through reduction in carrier mobility.

Noise and electromagnetic interference are concerns at lower drain currents, where the device becomes very resistive having $1/g_m$ in the 100s of kΩ. For currents below 1 µA, ten samples were taken for each data point for preprocessing. The preprocessing, implemented in MATLAB, would take either the median or mean of these ten samples. The difference between median and mean preprocessing was small. When data was preprocessed using the median of the ten current points, the overall error between experimental and model data was smaller than when processed with the mean. While white noise is a zero-mean stochastic process, the attempt at reducing its impact through an ensemble average was not very effective. This could be from taking only ten samples. With more samples, the mean preprocessing might work better than the median.

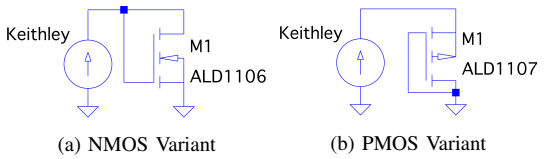

(a) NMOS Variant (b) PMOS Variant

Fig. 1: Circuits Topologies used for Measuring of MOSFET I-V Dependence

III. Tuning of the Modified ACM Expression

This section deals with selecting V_{norm}, I_{norm}, and m in (5) to optimize the fit with experimental data.

The fact that the model is in I-g_m domain, while the experimental data are in I-V domain, complicates the tuning task. To match model and experiment, we perform a 'domain conversion'. One could convert experimental data from I-V to I-g_m domain to compare transconductance values. Fig. 2 clarifies this approach. Alternatively, as depicted in Fig. 3, one could convert the model-generated I-g_m data to I-V domain and perform a comparison of voltage values. Both approaches are employed in this paper because we want to show that (5) is robust, where its parameters are not particularly sensitive to the tuning strategy used.

A. Tuning by Comparing Transconductance Values

Extracting and verifying an I-g_m model from measured I-V data requires differentiation typically approximated with forward or backward differences.

Because this study relies on the accuracy of the first derivative, a formula based on quadratic spline interpolation of the data was used instead. The quadratic spline interpolation takes three points and assumes a quadratic function passes through the three points. The derivative of this quadratic at the center point is assumed to be the first derivative of the nonlinear function. Following this idea, we derived (6).

$$g_m \cong \frac{I_{D(k)} - I_{D(k-1)}}{V_{GS(k)} - V_{GS(k-1)}} + \frac{I_{D(k+1)} - I_{D(k)}}{V_{GS(k+1)} - V_{GS(k)}} - \frac{I_{D(k+1)} - I_{D(k-1)}}{V_{GS(k+1)} - V_{GS(k-1)}} \quad (6)$$

Expression (6) generalizes the simpler two-point differences. It uses all three differences one could form between three points and guarantees zero error for both linear and quadratic dependencies.

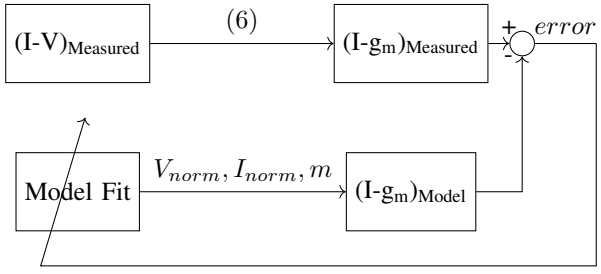

Fig. 2: Fitting Algorithm that Reduces Error in I-g_m Domain

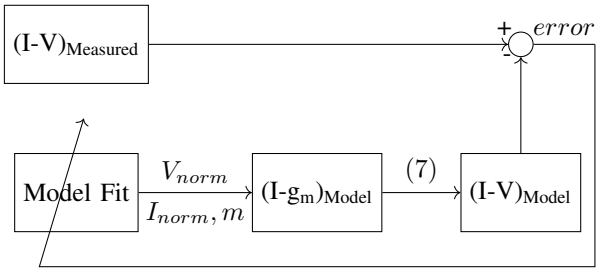

Fig. 3: Fitting Algorithm that Reduces Error in I-V Domain

B. Tuning by Comparing V_{GS} Values

Equation (6) generates I-g_m points from the experimental I-V set. As such, it does not offer a direct comparison to measured data. Also, the derivative operator (6) may enhance errors present in the measured data. To circumvent this issue, we also consider the tuning strategy of Fig. 3 - an approach based upon (7). Expression (7) derives from (6) and allows us to produce an I-V set from an I-g_m one. It can be thought an integral operation.

$$V_{GS(k+1)} \cong V_{GS(k)} + 2\frac{I_{D(k+1)} - I_{D(k)}}{g_{m(k+1)} - g_{m(k)}} \tag{7}$$

The tuning strategy in Fig. 3 provides direct comparison to measured data and offers more intuition on how accurately the model matches the actual measurements.

C. Selecting a Cost Function to Minimize

We calculate the error by taking the absolute value of the difference between each experimental and model value and dividing it by the corresponding experimental value. Depending on the tuning strategy used, the error calculation involves either g_m values or V_{GS} values, but the normalization ensures the error is always a dimensionless quantity.

Our measured and model-produced data sets consist of N points (N $>$ 150). Hence, the error could be seen as an N-dimensional vector **e** and the tuning process as an effort to minimize the 'length' of the vector. According to [7], the length of an N-dimensional vector in R_N space is its norm (8).

$$||\mathbf{e}||_p = \left(\sum_{i=1}^{N} e_i^p \right)^{\frac{1}{p}}, \quad p \geq 1 \tag{8}$$

The most common norms are the grid norm (p=1), the Euclidean norm (p=2), and the infinity norm (p=∞). In this study, we choose to work with l_1 and l_∞ not only because they represent the two ends of the spectrum but also because they have meaningful interpretations. As seen in (9) and (10), the average error relates to l_1 whereas the maximum error equals l_∞.

$$e_{ave} = \frac{e_1 + e_2 + ... + e_n}{n} \equiv \frac{||\mathbf{e}||_1}{N} \tag{9}$$

$$e_{max} = max\{e_1, e_2, ..., e_N\} \equiv ||\mathbf{e}||_\infty \tag{10}$$

Minimizing the Euclidean (l_2) norm, not pursued here, should perform between the 1-norm and the infinity-norm.

D. Defining the Search Space

To find the optimal model, we test various combinations of V_{norm}, I_{norm}, and m against experimental data. Reducing the number of cases tried requires establishing a meaningful range for each parameter. The considerations are provided below.

Because the transconductance in deep sub-threshold is given by I_D/V_{norm}, an approximate value for V_{norm} is easily obtained by finding the g_m at low currents and taking the ratio I_D/g_m. In this study, one hundred possible normalization voltages are taken from a ten percent window around the calculated approximate value of V_{norm}.

The normalization current, I_{norm}, delineates weak inversion from strong inversion. Examination of the experimental data for our devices reveals that this transition occurs at current levels below $10\,\mu A$. Thus, we took 100 evenly spaced current values between 0 and $10\,\mu A$.

Ideally, the optimum parameter search will return an m value of 0.5, validating (2), but larger values for m are also likely. As discussed in [3], m values in the range of 0.7 to 1 are common for sub-$0.5\,\mu m$ MOSFETs. This justifies a search range of 0.5 to 1. We again take 100 m values evenly spaced between 0.5 and 1.

With each parameter having 100 possible values, the tuning algorithm examines one million possible solutions. The one yielding the lowest error is kept and passed as the model fit output. For each transistor, we have four 'best' models corresponding to four possible combinations of two tuning schemes and two cost functions. The differences are discussed in the next section.

IV. Results and Discussion

A. Performance of Original and Modified ACM

As seen in Table II and III, the best fit is achieved with m values of approximately 0.6. This is true for both the n-channel and the p-channel devices. The exponent value changes little with change in tuning strategy and cost function.

Fig. 4 and 5 show that a model with m=0.5 fits the data poorly. This finding is surprising, considering the devices have a channel length of $7.8\,\mu m$.

B. Impact of Cost Function

Fig. 4 and 5 show that minimizing the mean error, i.e. using an l_1-based cost function, provides a better fit for lower current data points. This stems from a higher concentration of data points at lower currents that shifts the model fit to optimize lower currents. The higher current points suffer more error. Conversely, reducing the maximum error (l_∞) provides a better fit for higher current data points at the expense of lower current points. In absence of outliers, the discrepancies between the two cost functions should diminish if the density of the points is more uniform.

C. Impact of Tuning Domain

Table II and III show the tuning domain in this particular study has little impact upon optimum models found. General trends are intuitive and summarize as follows: optimizing in one domain sacrifices performance in the other domain. However, the differences are insignificant. We note that irrespective of tuning domain used, the V_{GS} error is small. Maximum error never exceeds 3.6%, and average error stays below 0.2%. The match between experimental g_m and modified ACM model typically has maximum error of 20-25% and an average of sub-10%. This performance is superior to the performance of the original ACM, where the maximum error exceeds 150%.

D. Differences Between N and P-Channel Devices

Tables II and III show differences between NMOS and PMOS devices. The devices have similar normalization voltages and m parameters, but their normalization currents are vastly different. ALD1106 has much larger I_{norm}. This larger I_{norm} does not stem from a wider n-channel transistor, as both devices have $138\,\mu m$ widths [4]. Referring to (3), the larger normalization current of ALD1106 can be explained by the higher mobility of electrons and the slightly larger n factor of ALD1106. The larger n is inferred from the larger V_{norm}.

V. Conclusion

This study shows the 'deviation from square-law' is not an exclusive attribute to sub-micrometer MOSFETs. As seen with the ALD1106 and ALD1107, a device with length of $7.8\,\mu m$ could exhibit 'high-field' effects sufficient to invalidate the ACM model. More importantly, the experimental results corroborate the argument presented in [3]. Namely, the I-g_m dependence of practical MOSFETs can be captured by a simple modification to the ACM. The introduced exponent m, a 'catch-all' parameter, accounts for many phenomena that shape the I-g_m dependence at high currents. These are strong vertical and lateral fields and finite source-side contact resistance among others. As such, the modified ACM offers analog designers an insight into the overall behavior of the device and facilitates biasing decisions.

TABLE II: MODEL PARAMETERS AND PERFORMANCE OF MODIFIED ACM EXTRACTED FROM ALD1106 MEASUREMENTS

Tuning Scheme		V_{norm}	I_{norm}	m	g_m Error, %		V_{GS} Error, %	
Domain	Cost Func.	[mV]	[µA]	-	max	average	max	average
g_m	l_∞	42.0	1.85	0.611	12.1	5.4	3.53	0.17
g_m	l_1	39.7	1.27	0.581	24.8	3.9	2.37	0.14
V	l_∞	40.6	1.85	0.601	26.4	9.7	0.79	0.14
V	l_1	40.1	1.47	0.586	27.9	5.5	1.39	0.13

TABLE III: MODEL PARAMETERS AND PERFORMANCE OF MODIFIED ACM EXTRACTED FROM ALD1107 MEASUREMENTS

Tuning Scheme		V_{norm}	I_{norm}	m	g_m Error, %		V_{GS} Error, %	
Domain	Cost Func.	[mV]	[µA]	-	max	average	max	average
g_m	l_∞	33.0	0.307	0.586	10.6	7.8	2.43	0.15
g_m	l_1	35.0	0.408	0.586	19.1	3.0	0.83	0.10
V	l_∞	38.1	0.509	0.596	22.2	3.7	0.59	0.09
V	l_1	36.8	0.509	0.601	19.4	3.3	0.72	0.08

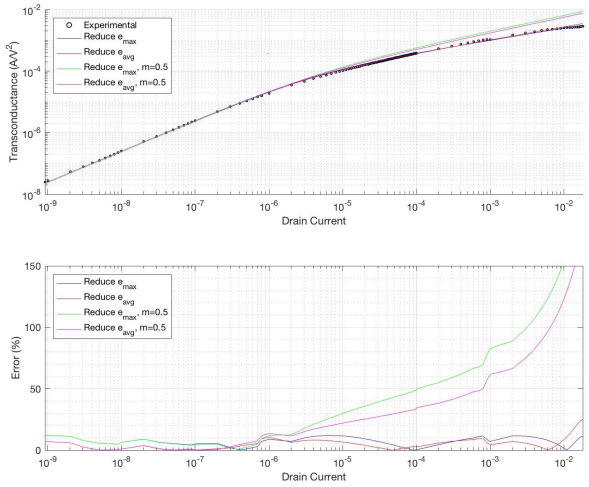

Fig. 4: ALD1106 experimental transconductance compared to modified ACM extracted using g_m-domain tuning and two different cost functions. The graphs also show the poor fit provided by the ACM (m=0.5).

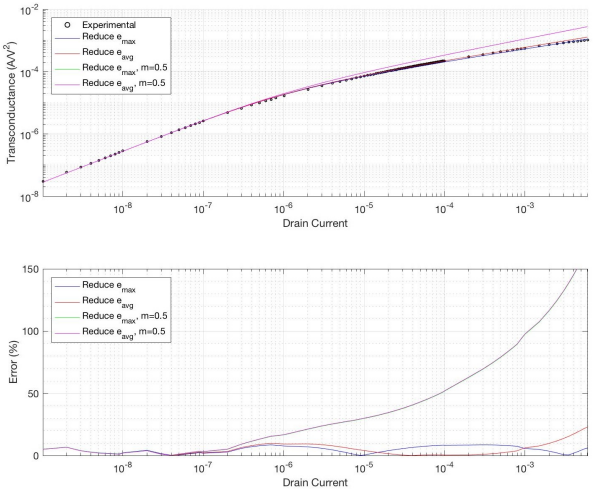

Fig. 5: ALD1107 experimental transconductance compared to modified ACM extracted using g_m-domain tuning and two different cost functions. The graphs also show the poor fit provided by the ACM (m=0.5).

References

[1] A. I. A. Cunha, M. C. Schneider, and C. Galup-Montoro, "An MOS transistor model for analog circuit design," *IEEE J. Solid-State Circuits*, vol 33, no. 10, pp. 1510-1519, October 1998.

[2] P. R. Gray, P. J. Hurst, S. H. Lewis, and R. G. Meyer, Analysis and Design of Analog Integrated Circuits, 4th ed., John Wiley & Sons, 2001, pp. 59.

[3] V. I. Prodanov, "Empirical model for the transconductance-current dependence of short-channel MOSFETs," 2012 IEEE 55th International Midwest Symposium on Circuits and Systems (MWSCAS), Boise, ID, 2012, pp. 290-293.

[4] Advanced Linear Devices, "ALD 11xx MOSFET PSPICE MODEL," ALD1106 and ALD1107 SPICE Models, Feb. 2004. [Online]. Available: http://aldinc.com/pdf/Model_ALDMOSFET.zip. [Accessed February 9, 2018].

[5] Advanced Linear Devices, "QUAD/DUAL P-CHANNEL MATCHED PAIR MOSFET ARRAY," ALD1107 datasheet, 2012.

[6] Advanced Linear Devices, "QUAD/DUAL N-CHANNEL MATCHED PAIR MOSFET ARRAY," ALD1106 datasheet, 2012.

[7] D. C. Lay, S. R. Lay, and J. J. McDonald, Linear Algebra and Its Applications, 5th ed., Pearson Education, Inc., 2016, pp. 379.